

# Palladium nanoclusters decorated partially decomposed porous ZIF-67 polyhedron with ultrahigh catalytic activity and stability on hydrogen generation



Chongbei Wu <sup>a,1</sup>, Jingya Guo <sup>a,1</sup>, Jifang Zhang <sup>a</sup>, Yanchun Zhao <sup>a, \*\*</sup>, Jianniao Tian <sup>a</sup>, Tayirjan Taylor Isimjan <sup>b, \*\*\*</sup>, Xiulin Yang <sup>a, \*</sup>

<sup>a</sup> Key Laboratory for the Chemistry and Molecular Engineering of Medicinal Resources (Ministry of Education of China), College of Chemistry and Pharmacy, **Guangxi Normal University**, Guilin 541004, PR China

<sup>b</sup> Saudi Arabia Basic Industries Corporation (SABIC) at King Abdullah University of Science and Technology (KAUST), Saudi Arabia

## ARTICLE INFO

### Article history:

Received 18 March 2018

Received in revised form

6 July 2018

Accepted 20 September 2018

Available online 21 September 2018

### Keywords:

Metal-organic frameworks

Partially decomposed

Pd nanoclusters

Hydrogen generation

Synergetic effect

## ABSTRACT

Metal-organic frameworks have attracted extensively attentions due to their unique structural properties such as high porosity, good crystallinity, and three-dimensional networking. However, to the best of our knowledge, there is no report concerning the application of partially decomposed metal-organic frameworks based catalyst for sodium borohydride hydrolysis for H<sub>2</sub> generation. Herein, the partially decomposed cobalt-based zeolitic imidazolate frameworks supported Pd nanoclusters are fabricated by evaporation solvent assisted method followed by subsequent annealing under H<sub>2</sub> atmosphere. Our results show that catalytic performance of the designed catalyst can be largely improved by optimizing the Pd loading and the annealing temperatures. The optimized catalyst exhibits a high catalytic activity towards hydrolysis of alkalinized sodium borohydride with a specific H<sub>2</sub> generation rate of 20.6 l min<sup>-1</sup> mg<sup>-1</sup> and turnover frequency of 495.0 mol min<sup>-1</sup> mol<sup>-1</sup> at 25 °C, which is the highest reported so far among the similar catalysts. Moreover, the resulted catalyst also demonstrates a high level of stability. Based on structural characterization and experimental optimization, the extraordinary performance of the fabricated catalyst is mainly contributed to the synergetic effect of highly dispersed Pd nanoclusters with partially decomposed cobalt-based zeolitic imidazolate frameworks.

Crown Copyright © 2018 Published by Elsevier Ltd. All rights reserved.

## 1. Introduction

Hydrogen is considered as one of the most promising sustainable energy sources due to the high chemical energy density [1–3]. However, the conventional hydrogen storages methods such as gas compression or liquefaction cannot meet the high-energy demand of automobile industry due to the relatively low storage density [4]. Accordingly, many works have been done to find high energy density hydrogen storage methods [5–8]. Sodium borohydride (NaBH<sub>4</sub>) is studied extensively due to the high theoretical hydrogen storage capacity (10.8%), easy-to-process and environmental

friendly, which makes it a good candidate for portable hydrogen generator [9–11]. Over past decades, the noble metal based catalysts were reported with a particularly high efficiency in terms of rapid hydrogen generation from NaBH<sub>4</sub> solution, such as Pt/CeO<sub>2</sub>–Co<sub>7</sub>Ni<sub>2</sub>O<sub>x</sub> [12], Pt/3D SiC [13], Pt/Co<sub>3</sub>O<sub>4</sub> [14], Pt/LiCoO<sub>2</sub> [15], Rh/Ni BNPs [16], Co<sub>0.8</sub>–Ag<sub>0.2</sub>–B [17], Ni/Au/Co [18], Ni<sub>0.9</sub>Pt<sub>0.1</sub>/Ce<sub>2</sub>O<sub>3</sub> [19], Ru@SiO<sub>2</sub> [20], and Ag/SiO<sub>2</sub>–CoFe<sub>2</sub>O<sub>4</sub> [21]. However, owing to the high cost of noble metals and self-agglomeration, transition metal based catalysts would be a desirable alternative [22–24]. Recently, many non-noble transition metal catalysts have been investigated in this regards but most of the results are unsatisfactory due to the low activity and poor reusability [25,26]. Another alternative approach is to improve the catalyst support to improve catalyst dispersion and decrease the catalyst loading [27,28]. As a result, the price of the noble metals will not be an issue. In this regards, metal-organic frameworks (MOFs) supported noble metal catalysts have attracted broadly attention due to their high surface areas, tunable porosities and thermal stability [29]. It has been well

\* Corresponding author.

\*\* Corresponding author.

\*\*\* Corresponding author.

E-mail addresses: [yanchunzhao@aliyun.com](mailto:yanchunzhao@aliyun.com) (Y. Zhao), [isimjant@sabic.com](mailto:isimjant@sabic.com) (T.T. Isimjan), [xiulin.yang@kaust.edu.sa](mailto:xiulin.yang@kaust.edu.sa) (X. Yang).

<sup>1</sup> These authors contributed equally.

accepted that the confined pores and cavities of MOFs define the anchored metal particles sizes and distribution, which in turn not only improve the catalytic activity, but also inhibit particle migration and aggregation, consequently enhance the catalyst stability in the hydrolysis process [30,31]. So far, a series of metal particles/MOFs catalysts have been developed for hydrolytic H<sub>2</sub> generation, e.g., Pd@MIL-101 [32], PdNi@MIL-101 [33], AgPd@UIO-66-NH<sub>2</sub> [34], RhNi@ZIF-8 [35], Pt@MIL-101 [36], Ru@MIL-53 [37], Ru@MIL-96 [38], and so on. But the TOF values of most catalysts for NaBH<sub>4</sub> hydrolysis are between 80 and 270 min<sup>-1</sup>. In general, most of the MOFs used as supports have very low conductivity thereof hindering charge transfer process during the hydrolysis, thereby significantly reducing the catalytic activity. Furthermore, the current knowledge on the reaction mechanism of MOF supported noble metal catalyst for NaBH<sub>4</sub> hydrolysis remains rather limited and unclear.

Herein, we designed and synthesized partially decomposed cobalt-based zeolitic imidazolate frameworks supported Pd catalyst (Pd/PD-ZIF-67) for NaBH<sub>4</sub> hydrolysis that exhibits high level of structural stability, good conductivity and well-dispersed active sites. Accordingly, the optimized Pd/PD-ZIF-67 catalyst shown the highest catalytic activity so far reported among the metal/MOF catalyst for H<sub>2</sub> generation with a TOF value of 495.0 mol min<sup>-1</sup> mol<sup>-1</sup><sub>Pd</sub> toward hydrolysis of NaBH<sub>4</sub> at 25 °C. Additionally, the Pd/PD-ZIF-67 catalyst also displayed remarkable stability on the NaBH<sub>4</sub> hydrolysis for H<sub>2</sub> generation with a minimum decay of catalytic activity around 10% after five consecutive cycles. The superior catalytic performance could be ascribed to the partial oxidation of Co induced fast electron transfer property and high level of hydrophilicity that synergistically combined with the highly dispersed Pd nanoclusters thereof enhances the catalytic activity. Accordingly, we proposed a possible catalytic mechanism.

## 2. Experimental

### 2.1. Synthesis of Pd/PD-ZIF-67

All chemical reagents are analytical grade and used without further purification. ZIF-67 was prepared by a solution precipitation method (Fig. S1) [39]. The hybrid material of Pd/PD-ZIF-67 was achieved by the following two steps. Initially, 50 mg of as-synthesized ZIF-67 was ultrasonically dispersed into 10 mL of acetone for 20 min. After that, a certain amount of Pd(NO<sub>3</sub>)<sub>2</sub> aqueous solution (10 mg mL<sup>-1</sup>) was added into the above solution under vigorous stirring at room temperature. After continuous stirring for another overnight, the acetone was evaporated and the remaining solids were collected. Then, the collected solid was finely ground to a fine powder before being put into a tube furnace. The heating temperatures slowly rise to the target temperatures (150 °C–350 °C) at a fixed heating rate of 2 °C min<sup>-1</sup> in H<sub>2</sub> atmosphere for 2 h. After cooling to ambient temperature, the resulted Pd/PD-ZIF-67 hybrid materials were obtained for subsequent use.

### 2.2. Catalyst characterizations

The morphologies and microstructures of the catalysts were characterized by scanning electron microscope (SEM, FEI Quanta 200 FEG) and transmission electron microscope (TEM, JEM-2100F). The crystal structures of different catalysts were analyzed by X-ray powder diffraction (XRD, Rigaku D/Max 2500 V/PC) with a sweep speed for 5.0° min<sup>-1</sup>. The X-ray photoelectron spectrometer (XPS, JPS-9010 Mg K $\alpha$ ) was used to analyze of the chemical states of different elements in the hybrid materials. The actual metal loading

of different metals in the composite were detected by inductive coupled plasma emission spectrometer (ICP, IRIS IntrepidII XSP). The conductivity of the synthesized materials were measured by a four-probe system (RTS-2A).

### 2.3. Catalytic measurements

The synthesized catalysts of catalytic performance, reusability and activation energy were studied as following. Initially, 50 mL of 150 mM NaBH<sub>4</sub> (contained 0.4 wt% NaOH) was injected into a round-bottomed flask (100 mL) and continuously stirred for 0.5 h at 25 °C in water bath heater. After that, 10 mg catalyst was added into the above solution. The produced H<sub>2</sub> was calculated by a drainage method, in which the overflowed water was collected and weighted by a balance. The instantly changed qualities of water were recorded by a computer which had connected with the used balance. The reusability procedures of the catalyst were described as following. The above hydrolyzed solution of NaBH<sub>4</sub> was stirred for another 1 h for the completed reaction in the first-cycle, and then the catalytic procedure of NaBH<sub>4</sub> hydrolysis was repeated and detected the H<sub>2</sub> generation again using the same amount of NaBH<sub>4</sub>. The activation energy of the designed catalyst was evaluated by research at different temperatures in the same device including 25 °C, 30 °C, 35 °C, 40 °C and 45 °C.

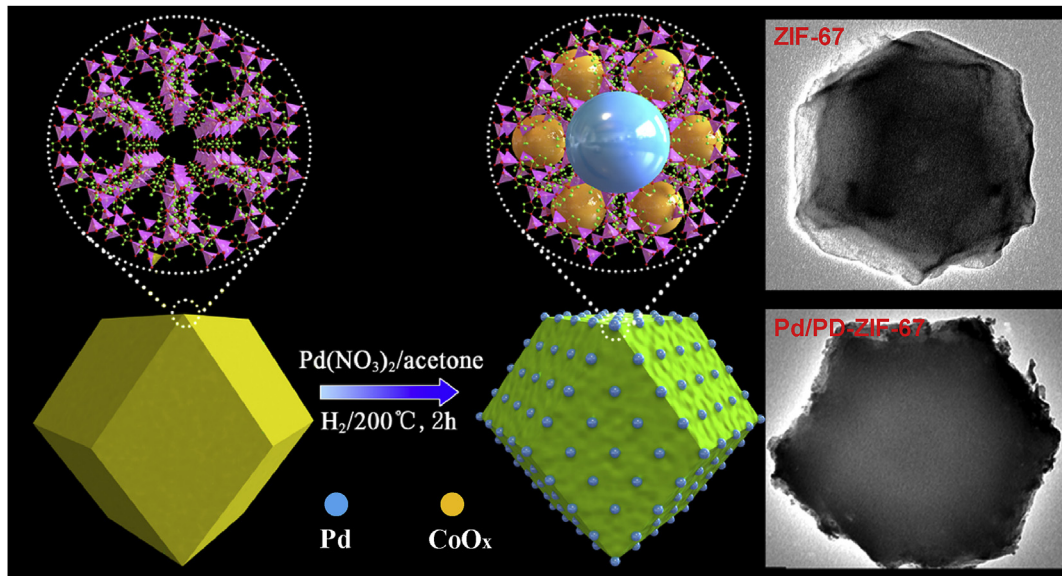
## 3. Results and discussion

### 3.1. Synthesis and characterizations of Pd/PD-ZIF-67

As a zeolitic imidazole framework (ZIF), the ZIF-67 was selected because it can be rapidly synthesized with commercial available reagents, thermally stable and highly porosity [40]. The Pd/PD-ZIF-67 nanocomposites are prepared by dispersing the ZIF-67 particles in the acetone solution of Pd(NO<sub>3</sub>)<sub>2</sub> followed by slow evaporation of the solvent. The resulting mixture was subsequently calcined in the H<sub>2</sub> atmosphere for 2 h. The schematics are shown in Scheme 1. The optimal performance of the catalyst was obtained 1.62 wt% Pd loading at the reduction temperature of 200 °C.

The crystal structures of the synthesized Pd/PD-ZIF-67 materials at different temperatures along with ZIF-67 are characterized by X-ray diffraction (XRD) patterns. As shown in Fig. 1a, the Pd/PD-ZIF-67 (200 °C) exhibits several additional peaks compared to the that of pure ZIF-67 [41]. Whereas the peaks at 19.0, 31.2, 36.8, 38.6, 44.7, 55.6, 59.3 and 65.1° can be ascribed to the cubic structures of Co<sub>3</sub>O<sub>4</sub> (JCPDS: 43-1003) [42], while the peaks at 42.3, 61.5, 73.7 and 77.3° are due to the cubic structures of CoO (JCPDS: 43-1004). The peaks at 40.1, 46.7, 68.4 and 82.3° are attributed to the cubic crystal of (111), (200), (220) and (311) facets of Pd (JCPDS: 46-1043) [43,44]. Other than these features, the rest of the peaks are perfectly overlapped with these of ZIF-67. However, when the reduction temperatures are equal to or higher than 250 °C, the diffraction peaks of ZIF-67 in the hybrid materials are all disappeared and all the Co-species were transformed into CoO<sub>x</sub> (Fig. S1), meaning the Pd/PD-ZIF-67 can be decomposed at the annealing temperature higher than 200 °C (Fig. S2). The morphologies of Pd/PD-ZIF-67 start to collapse from 200 °C indicating that the partial decomposition becomes visible after 200 °C.

The microstructures of ZIF-67 and the corresponding Pd/PD-ZIF-67 were investigated by scanning electron microscope (SEM) and transmission electron microscopy (TEM). As shown in Fig. 1b and c, the SEM images of the ZIF-67 exhibits clear edges and well-defined structures. After Pd deposition, the new catalyst Pd/PD-ZIF-67 still kept the rhombic dodecahedron crystal morphology of ZIF-67, but the surface became relatively rough compared to that of ZIF-67 (Fig. 1d and e). The TEM image shows well-dispersed Pd



**Scheme 1.** Schematic synthesis of Pd nanoclusters on PD-ZIF-67 support by a facile evaporation method combined with a subsequent H<sub>2</sub>-assisted reduction treatment.

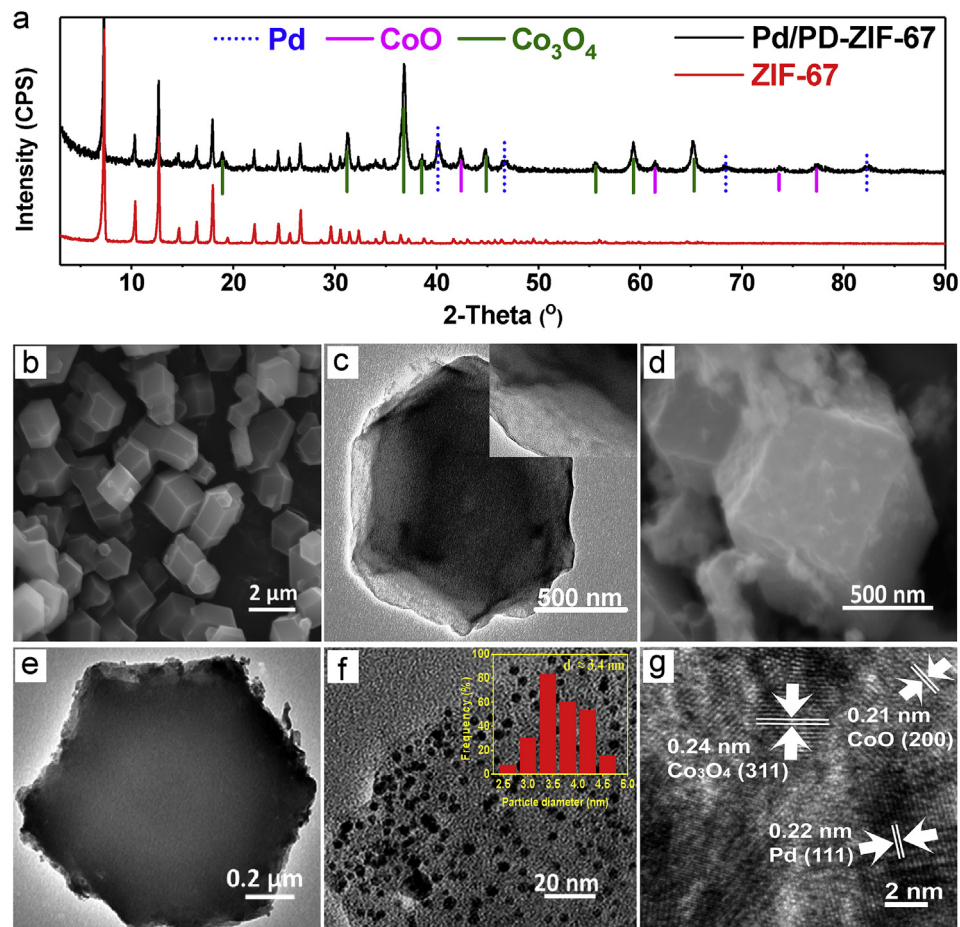


**Fig. 1.** (a) XRD patterns of synthesized ZIF-67 and Pd/PD-ZIF-67. (b) SEM image and (c) TEM image of ZIF-67. (d) SEM image of Pd/PD-ZIF-67. (e,f) TEM images of Pd/PD-ZIF-67 with different magnifications. (g) High-resolution TEM image of Pd/PD-ZIF-67.

nanoclusters with the size distribution between 2.4 and 4.8 nm, and the average particle size is 3.4 nm (Fig. 1f). The Pd nanoclusters start to agglomerate when the annealing temperature under H<sub>2</sub> is increased to 300 °C and a clear agglomeration can be visualized by

TEM (Fig. S3). The three different lattice d-spacings with the value of 0.24, 0.21 and 0.22 nm correspond to the Co<sub>3</sub>O<sub>4</sub> (311), CoO (200) and Pd (111) respectively, which clearly indicates the coexistence of these three components in the Pd/PD-ZIF-67 treated at 200 °C for

2 h (Fig. 1g). The mapping of energy dispersive spectroscopy (EDS) reveals the uniform distributions of the Co, Pd, O, N and C species on the Pd/PD-ZIF-67 surface (Fig. S4). Moreover, the actual loadings of Pd species in hybrid materials (200 °C) are determined by ICP and the results are consistent with the experimental values (Table S1).

The elemental compositions and chemical states of the Pd/PD-ZIF-67 (200 °C) are also determined by X-ray photoelectron spectroscopy (XPS). The XPS survey spectrum revealed the Pd, Co, N, O and C elements in Pd/PD-ZIF-67 composite as shown in Fig. S5 and the high resolution C 1s XPS spectrum is convoluted into C=C (284.0 eV), C-C (284.8 eV) and C-O (286.0 eV), respectively [39]. The high-resolution Pd 3d spectrum is analyzed by fitting into six asymmetric peaks (Fig. 2a), whereas the peaks are assigned according to the literature on Pd 3d<sub>5/2</sub>. The Pd 3d<sub>5/2</sub> three doublets at 335.2, 336.8 and 338.6 eV are corresponding to metallic Pd, adsorbed Pd<sup>2+</sup> and PdO, respectively [45]. The relative contents of the metallic Pd, adsorbed Pd<sup>2+</sup> and PdO are 20.9%, 16.4% and 62.7% in the total Pd, respectively. Fig. 2b shows the high-resolution Co 2p spectrum, where the characteristic peaks of metallic Co<sup>0</sup> locate at 778.8 eV (2p<sub>3/2</sub>), while the binding energies at 780.3 eV (2p<sub>3/2</sub>) and 795.7 eV (2p<sub>1/2</sub>) and their corresponding satellites are due to Co<sup>3+</sup>/Co<sup>2+</sup> [46]. The two peaks corresponding to N 1s appear at 398.6 and 400.1 eV (Fig. 2c), which are ascribed to pyridinic-N and pyrrolic-N [47], respectively.

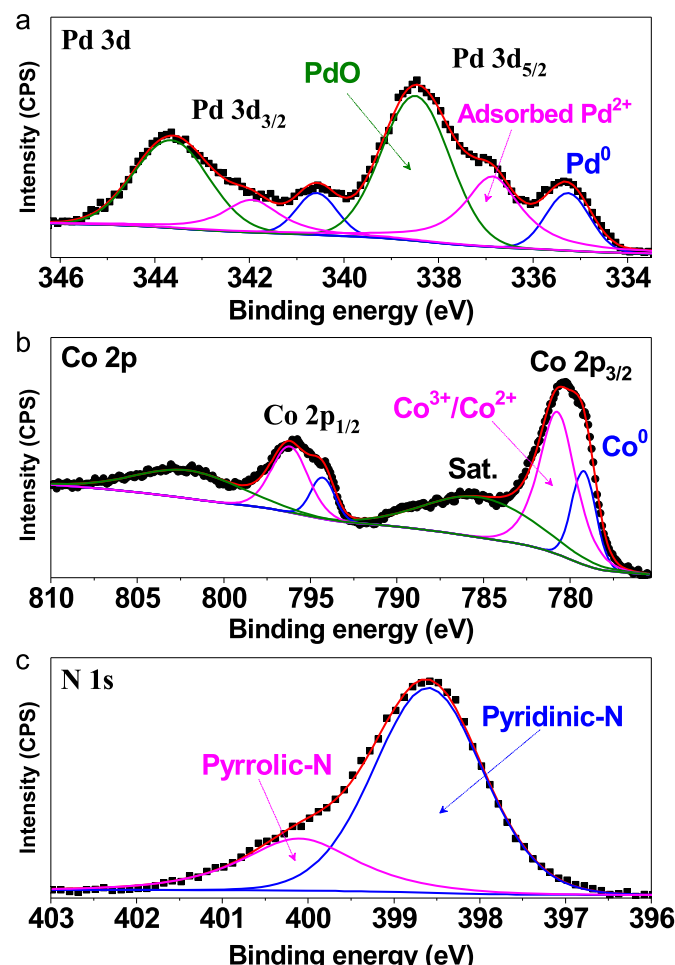


**Fig. 2.** High-resolution XPS spectra and corresponding peak convolutions of (a) Pd 3d, (b) Co 2p and (c) N 1s from Pd/PD-ZIF-67 material ( $\text{H}_2$ , 200 °C, 1.62 wt% Pd).

### 3.2. Catalytic hydrolysis analysis

A series of Pd/PD-ZIF-67 catalysts with various compositions have been applied to hydrolytic dehydrogenation of NaBH<sub>4</sub> at ambient temperature under the alkaline condition in which the concentration of NaBH<sub>4</sub> is 150 mM and mass fraction of NaOH is 0.4 wt%. The schematic illustration of the setup is shown in Fig. S6 for better understanding the experimental process. Initially, we performed quick screening experiments according to the anticipated Pd loadings which could be somewhere around 1 to 2 wt%, therefore Pd loading of 1.62 wt% was used to optimize the effect temperature on the catalytic activities of Pd/PD-ZIF-67. The catalytic performance of the Pd/PD-ZIF-67 varies with the changing reduction temperatures from 150 °C to 350 °C (Fig. 3a and b). When the reduction temperature reaches 200 °C, the specific H<sub>2</sub> generation rate and TOF reach the maximum value of 20.6 L min<sup>-1</sup> mg<sub>Pd</sub><sup>-1</sup> and 495.0 mol min<sup>-1</sup> mol<sub>Pd</sub><sup>-1</sup>, respectively. The changes in catalytic performance of Pd/PD-ZIF-67 at various temperatures could be due to following two reasons. First of all, under the lower temperature (<200 °C), the catalyst conductivity is very low due to the lack of CoO<sub>x</sub> species in the system (Fig. S1). Notably, the conductivity of Pd/PD-ZIF-67 (200 °C) is around 0.058 S cm<sup>-1</sup> by a four-probe measurement, which is significantly higher than that of pure ZIF-67 (0.025 S cm<sup>-1</sup>). As a result, the catalytic activity is low. On the other hand, the structure of the catalyst is destroyed and Pd is agglomerated at the higher temperature (>200 °C) (Fig. S1-S3). Hence, the optimal performance at 200 °C is the result of the direct interaction of above two main factors namely conductivity and structural integrity.

Furthermore, the effects of various Pd loadings on the Pd/PD-ZIF-67 on the hydrolysis of alkalinized NaBH<sub>4</sub> at optimal annealing temperature of 200 °C are further investigated. The results revealed that the specific H<sub>2</sub> generation rate (Fig. 3c) and TOF value (Fig. 3d) show parabolic behaviors where the maximum values of H<sub>2</sub> generation rate and TOF are obtained with 1.62 wt% Pd loading. The catalytic activities of various Pd loadings heavily altered by the agglomeration of Pd nanoclusters when sufficient active sites present on the support (Fig. S7). The optimal catalytic performance is not only significantly higher than these of the PD-ZIF-67, original ZIF-67 and commercial Pd/C catalysts (Fig. S8) but also is the best performance reported so far among the similar catalysts (Table S2).

The activation energy of the NaBH<sub>4</sub> hydrolysis in alkaline solution of the best performing Pd/PD-ZIF-67 is calculated using Arrhenius equation ( $k = A \cdot e^{-E_a/RT}$ ) in 150 mM NaBH<sub>4</sub> + 0.4 wt% NaOH solution and the reaction temperatures are varied from 25 °C to 45 °C as shown in Fig. 4a [48]. Where the  $k$  (L min<sup>-1</sup> g<sup>-1</sup>) is the specific H<sub>2</sub> evolution rate,  $E_a$  is the activation energy (kJ mol<sup>-1</sup>),  $R$  is the gas constant (8.314 J mol<sup>-1</sup> K<sup>-1</sup>) and  $T$  is the applied solution temperature (K). The plot of the lnk (rate constant) versus the inverse of the temperature as shown in Fig. 4b reveals straight line. The value of  $E_a$  is calculated according to the slope of the line, which is equal to  $E_a/R$ . The  $E_a$  of the best performing catalyst is estimated to be 58.5 kJ mol<sup>-1</sup>.

The stability of the optimized Pd/PD-ZIF-67 catalyst is evaluated by continuous recycle the experiment of NaBH<sub>4</sub> hydrolysis. The catalyst was cleaned and a fresh solution was used in each reaction cycle. The H<sub>2</sub> generation rates were decreased slightly after five cycles around 10% as shown in Fig. 4c and d. Interestingly, H<sub>2</sub> generation rate increases slightly at the third cycle compare to the first two cycles, which can be ascribed to the increase of the metallic Pd content from 20.9% to 59.2% as shown in XPS (Fig. S9) resulted from NaBH<sub>4</sub> reduction. On the other hand, the content of metallic Co is slightly increased (Fig. S10) due to the Pd–H assisted BH<sub>4</sub> reduction [49,50], and the metallic Co could also involve the

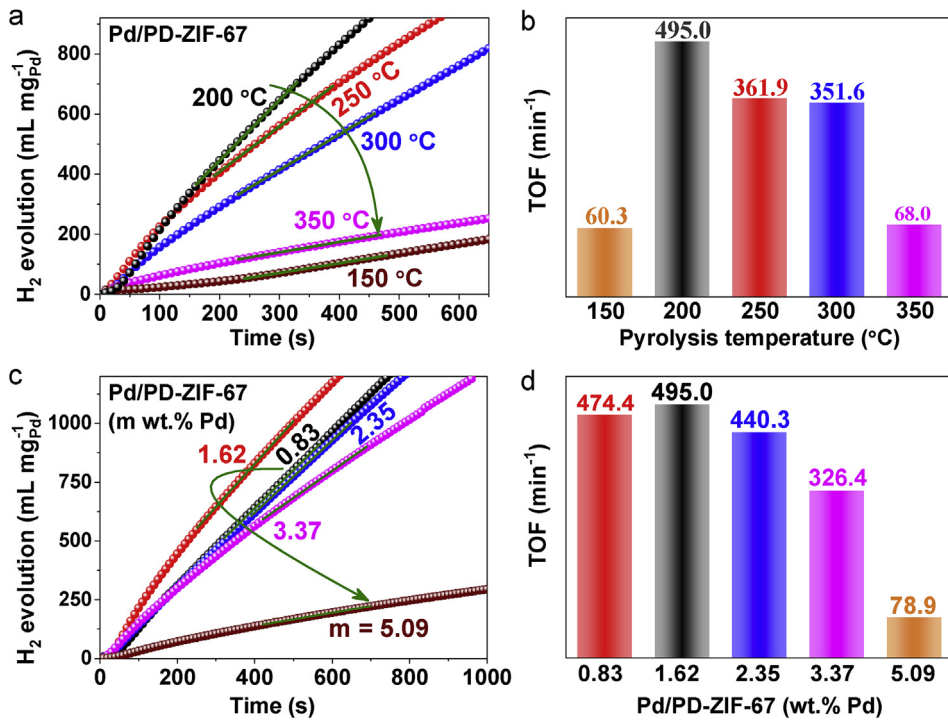


**Fig. 3.** (a) The effect of reduction temperatures on the synthesis of Pd/PD-ZIF-67 catalysts in H<sub>2</sub> atmosphere (1.62 wt% Pd) for H<sub>2</sub> generation from hydrolysis of 150 mM NaBH<sub>4</sub> + 0.4 wt% NaOH solution. (b) The TOF values are obtained from a. (c) The effect of Pd loadings on Pd/PD-ZIF-67 (H<sub>2</sub>, 200 °C) catalysts for H<sub>2</sub> generation by hydrolysis of alkalinized NaBH<sub>4</sub>. (d) The TOF values are summarized from c.

NaBH<sub>4</sub> hydrolysis as well [51]. Notably, the morphologies and structures of Pd/PD-ZIF-67 catalyst suffer a certain degree of decomposition after 5th cycles (Fig. S11). Therefore, the catalyst deactivation could be due to the Pd agglomerations, structural damages and catalyst poisoning by BO<sub>2</sub><sup>-</sup> species [52].

### 3.3. Catalytic mechanism analysis

As mentioned above, the Pd/PD-ZIF-67 (H<sub>2</sub>, 200 °C, 1.62 wt%) catalyst exhibits the highest specific H<sub>2</sub> evolution rate and TOF value, where the enhanced catalytic performance is defined by the

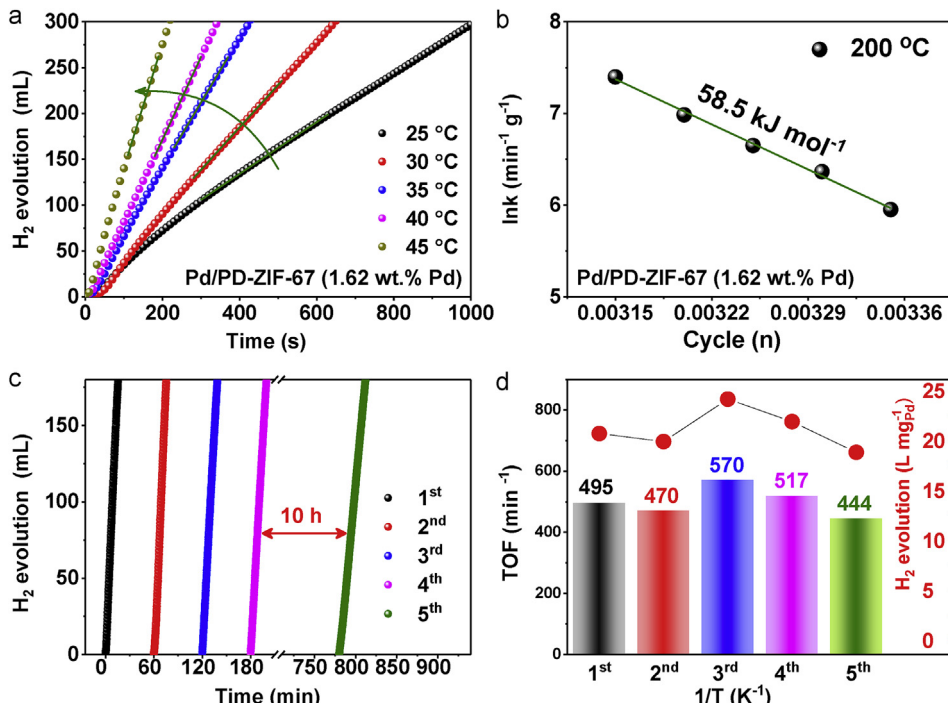


**Fig. 4.** (a) The effect of hydrolysis temperatures for H<sub>2</sub> production on the Pd/PD-ZIF-67 catalyst (H<sub>2</sub>, 200 °C, 1.62 wt% Pd) by hydrolysis of alkalinized NaBH<sub>4</sub> solution. (b) The summarized Arrhenius plot from c. (c) The reusability of Pd/PD-ZIF-67 catalyst (H<sub>2</sub>, 200 °C, 1.62 wt% Pd) for continuous hydrolysis of 150 mM NaBH<sub>4</sub> + 0.4 wt% NaOH solution. (d) The summarized TOF values and specific H<sub>2</sub> evolution from a.

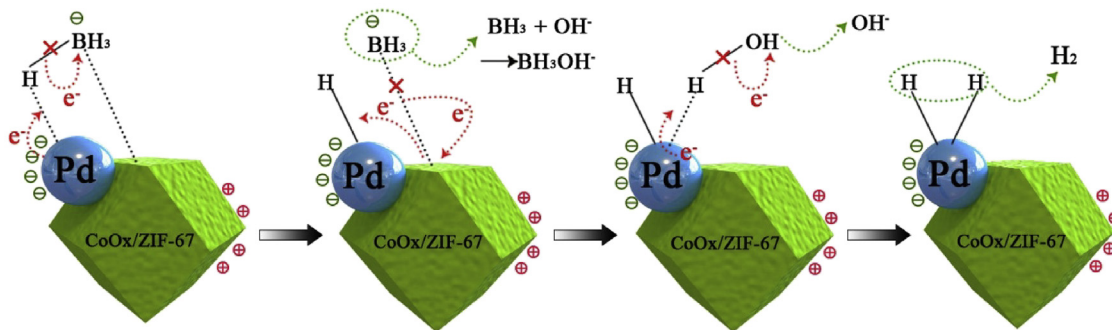


**Fig. 5.** Catalytic mechanism diagram of the Pd/PD-ZIF-67 catalyst for H<sub>2</sub> generation by hydrolysis of alkalized NaBH<sub>4</sub> solution.

synergistic effect of the particle size and size distribution of Pd nanoclusters, conductivity of the metal-organic frameworks resulted by the Co-oxide species. The experimental results show that the electron transfer to Pd can be enhanced considerably by altering the content of CoO<sub>x</sub> species in the ZIF-67. The actual reason is unknown to us at this stage. One may suggest that the partial oxidation of ZIF-67 could generate free NH groups on the surface that ready to be chelated with Pd<sup>2+</sup> subsequently improve the synergistic effect between the active sites and support thereof enhance catalytic activity. Moreover, the proposed mechanism is described in Fig. 5. The partial charge separation has resulted because of the different work functions of Pd, Co<sub>3</sub>O<sub>4</sub> and CoO, which are about 5.22, 4.5 and 3.7 eV respectively. Thus, the PD-ZIF-67 surface is partially positive while the Pd nanoclusters are partially negative (Fig. S12). As a result, the BH<sub>4</sub><sup>-</sup> ions are more inclined to adsorb onto the support whereas one of H belong to BH<sub>4</sub><sup>-</sup> ions will adsorb onto the active sites of Pd nanoclusters while the B is adsorbed by PD-ZIF-67 surface [53]. As the B–H bond breaks, Pd–H<sub>ads</sub> and PD-ZIF-67–(BH<sub>3</sub>)<sub>ads</sub> are promptly formed on the catalyst surface. After that, with the adsorbed BH<sub>3</sub><sup>-</sup> peels off, one electron will release onto the active sites of PD-ZIF-67 [54]. Due to the metallic property of Pd and good conductivity of the PO/ZIF-67, the electron can be quickly transferred to the Pd nanoclusters, and then interact with H<sub>2</sub>O molecules to form another Pd–H<sub>ads</sub>. Finally, the resulted neighboring Pd–H<sub>ads</sub> intermediates combine quickly and subsequently release H<sub>2</sub>. The BH<sub>4</sub><sup>-</sup> ions are eventually hydrolyzed to B(OH)<sub>4</sub><sup>-</sup> ions (B(OH)<sub>4</sub><sup>-</sup> ↔ BO<sub>2</sub><sup>-</sup> + 2H<sub>2</sub>O) after three cycles [55].

#### 4. Conclusion

In summary, a novel Pd/PD-ZIF-67 hybrid catalyst with low noble metal loading is developed by a solution deposition followed by a H<sub>2</sub>-assisted reduction method at 200 °C. The effects of the Pd loading and annealing temperatures on NaBH<sub>4</sub> hydrolysis are systematically optimized. The optimized catalyst of the Pd/PD-ZIF-67 (H<sub>2</sub>, 200 °C, 1.62 wt%) exhibits outstanding catalytic performance and high stability. The synergistic effects between different species of the hybrid catalyst as well as the improved conductivity of the support are proposed to be the two main factors that largely alter the catalytic performance of the Pd/PD-ZIF-67. Accordingly, we suggested possible reaction mechanism. These findings provide a mechanical insight in to the dynamics associated with Pd loading and support conductivity and hence offer valuable guidance for rational design of efficient catalyst for NaBH<sub>4</sub> hydrolysis.

#### Notes

The authors declare no competing financial interest.

#### Acknowledgments

This work has been supported by the National Natural Science Foundation of China (21363003, 21165004, 21163002), Natural Science Foundation of Guangxi Province (2014GXNSFGA118008, 2014GXNSFFA118003), BAGUI scholar program (2014A001) and Project of Talents Highland of Guangxi Province.

#### Appendix A. Supplementary data

Supplementary data to this article can be found online at <https://doi.org/10.1016/j.renene.2018.09.070>.

#### References

- X. Hao, Z. Jin, H. Yang, G. Lu, Y. Bi, Peculiar synergistic effect of MoS<sub>2</sub> quantum dots and graphene on Metal-Organic Frameworks for photocatalytic hydrogen evolution, *Appl. Catal. B Environ.* 210 (2017) 45–56.
- D. Liu, Z. Jin, Y. Bi, Charge transmission channel construction between a MOF and rGO by means of Co-Mo-S modification, *Catal. Sci. Technol.* 7 (2017) 4478–4488.
- Z. Jin, H. Yang, Exploration of Zr–Metal–Organic framework as efficient photocatalyst for hydrogen production, *Nanoscale Res. Lett.* 12 (2017) 539.
- S.-J. Li, Y. Ping, J.-M. Yan, H.-L. Wang, M. Wu, Q. Jiang, Facile synthesis of AgAuPd/graphene with high performance for hydrogen generation from formic acid, *J. Mater. Chem. 3* (2015) 14535–14538.
- H. Zhang, G. Xia, J. Zhang, D. Sun, Z. Guo, X. Yu, Graphene-tailored thermodynamics and kinetics to fabricate metal borohydride nanoparticles with high purity and enhanced reversibility, *Adv. Energy Mater.* 8 (2018) 1702975.
- W. Chen, L.Z. Ouyang, J.W. Liu, X.D. Yao, H. Wang, Z.W. Liu, M. Zhu, Hydrolysis and regeneration of sodium borohydride (NaBH<sub>4</sub>)-A combination of hydrogen production and storage, *J. Power Sources* 359 (2017) 400–407.
- J.-M. Yan, S.-J. Li, S.-S. Yi, B.-R. Wulan, W.-T. Zheng, Q. Jiang, Anchoring and upgrading ultrafine NiPd on room-temperature-synthesized bifunctional NH<sub>2</sub>-N-rGO toward low-cost and highly efficient catalysts for selective formic acid dehydrogenation, *Adv. Mater.* 30 (2018), 1703038.
- K.-H. Liu, H.-X. Zhong, S.-J. Li, Y.-X. Duan, M.-M. Shi, X.-B. Zhang, J.-M. Yan, Q. Jiang, Advanced catalysts for sustainable hydrogen generation and storage via hydrogen evolution and carbon dioxide/nitrogen reduction reactions, *Prog. Mater. Sci.* 92 (2018) 64–111.
- Q.-L. Zhu, Q. Xu, Liquid organic and inorganic chemical hydrides for high-capacity hydrogen storage, *Energy Environ. Sci.* 8 (2015) 478–512.
- J. Meng, C. Niu, L. Xu, J. Li, X. Liu, X. Wang, Y. Wu, X. Xu, W. Chen, Q. Li, Z. Zhu, D. Zhao, L. Mai, General oriented formation of carbon nanotubes from metal–organic frameworks, *J. Am. Chem. Soc.* 139 (2017) 8212–8221.
- L. Ouyang, W. Chen, J. Liu, M. Felderhoff, H. Wang, M. Zhu, Enhancing the regeneration process of consumed NaBH<sub>4</sub> for hydrogen storage, *Adv. Energy Mater.* 7 (2017), 1700299.
- C. Wu, J. Zhang, J. Guo, L. Sun, J. Ming, H. Dong, Y. Zhao, J. Tian, X. Yang, Ceria-induced strategy to tailor Pt atomic clusters on cobalt–nickel oxide and the synergistic effect for superior hydrogen generation, *ACS Sustain. Chem. Eng.* 6 (2018) 7451–7457.
- A. Lale, A. Wasan, R. Kumar, P. Miele, U.B. Demirci, S. Bernard, Organosilicon polymer-derived mesoporous 3D silicon carbide, carbonitride and nitride structures as platinum supports for hydrogen generation by hydrolysis of sodium borohydride, *Int. J. Hydrogen Energy* 41 (2016) 15477–15488.
- T.-F. Hung, H.-C. Kuo, C.-W. Tsai, H.M. Chen, R.-S. Liu, B.-J. Weng, J.-F. Lee, An alternative cobalt oxide-supported platinum catalyst for efficient hydrolysis of sodium borohydride, *J. Mater. Chem.* 21 (2011) 11754–11759.

- [15] Z. Liu, B. Guo, S.H. Chan, E.H. Tang, L. Hong, Pt and Ru dispersed on LiCoO<sub>2</sub> for hydrogen generation from sodium borohydride solutions, *J. Power Sources* 176 (2008) 306–311.
- [16] L. Wang, L. Huang, C. Jiao, Z. Huang, F. Liang, S. Liu, Y. Wang, H. Zhang, Preparation of Rh/Ni bimetallic nanoparticles and their catalytic activities for hydrogen generation from hydrolysis of KBH<sub>4</sub>, *Catalysts* 7 (2017) 25.
- [17] L. Wei, Z. Yuan, Effects of Ag doping on the catalytic performance of Co-B NPs for hydrolysis of alkaline sodium borohydride solution, in: AIP Conf. Proc., vol. 1794, 2017, 020004.
- [18] C. Jiao, Z. Huang, X. Wang, H. Zhang, L. Lu, S. Zhang, Synthesis of Ni/Au/Co trimetallic nanoparticles and their catalytic activity for hydrogen generation from alkaline sodium borohydride aqueous solution, *RSC Adv.* 5 (2015) 34364–34371.
- [19] H.-L. Wang, J.-M. Yan, Z.-L. Wang, S.-I. O, Q. Jiang, Highly efficient hydrogen generation from hydrous hydrazine over amorphous Ni<sub>0.9</sub>Pt<sub>0.1</sub>/Ce<sub>2</sub>O<sub>3</sub> nanocatalyst at room temperature, *J. Mater. Chem. I* (2013) 14957–14962.
- [20] Q. Yao, W. Shi, G. Feng, Z.-H. Lu, X. Zhang, D. Tao, D. Kong, X. Chen, Ultrafine Ru nanoparticles embedded in SiO<sub>2</sub> nanospheres: highly efficient catalysts for hydrolytic dehydrogenation of ammonia borane, *J. Power Sources* 257 (2014) 293–299.
- [21] J. Chen, Z.-H. Lu, Y. Wang, X. Chen, L. Zhang, Magnetically recyclable Ag/SiO<sub>2</sub>–CoFe<sub>2</sub>O<sub>4</sub> nanocomposite as a highly active and reusable catalyst for H<sub>2</sub> production, *Int. J. Hydrogen Energy* 40 (2015) 4777–4785.
- [22] K. Fan, Z. Jin, H. Yuan, H. Hu, Y. Bi, Construction of CuO-modified zeolitic imidazolate framework-9 for photocatalytic hydrogen evolution, *Chin. J. Catal.* 38 (2017) 2056–2066.
- [23] Y. Zhang, Z. Jin, A. Iuan, G. Wang, Charge transfer behaviors over MOF-5@g-C<sub>3</sub>N<sub>4</sub> with Ni<sub>x</sub>Mo<sub>1-x</sub>S<sub>2</sub> modification, *Int. J. Hydrogen Energy* 43 (2018) 9914–9923.
- [24] K. Fan, Z. Jin, G. Wang, H. Yang, D. Liu, H. Hu, G. Lu, Y. Bi, Distinctive organized molecular assemble of MoS<sub>2</sub>, MOF and Co<sub>3</sub>O<sub>4</sub>, for efficient dye-sensitized photocatalytic H<sub>2</sub> evolution, *Catal. Sci. Technol.* 8 (2018) 2352–2363.
- [25] N. Sahiner, A.O. Yasar, N. Aktas, Metal-free pyridinium-based polymeric ionic liquids as catalyst for H<sub>2</sub> generation from NaBH<sub>4</sub>, *Renew. Energy* 101 (2017) 1005–1012.
- [26] S.-J. Li, H.-L. Wang, J.-M. Yan, Q. Jiang, Oleylamine-stabilized Cu<sub>0.9</sub>Ni<sub>0.1</sub> nanoparticles as efficient catalyst for ammonia borane dehydrogenation, *Int. J. Hydrogen Energy* 42 (2017) 25251–25251.
- [27] J.M. Yan, Z.L. Wang, L. Gu, S.J. Li, H.L. Wang, W.T. Zheng, Q. Jiang, AuPd–MnO<sub>x</sub>/MOF–Graphene: an efficient catalyst for hydrogen production from formic acid at room temperature, *Adv. Energy Mater.* 5 (2015), 1500107.
- [28] Z.-L. Wang, J.-M. Yan, Y. Ping, H.-L. Wang, W.-T. Zheng, Q. Jiang, An efficient CoAuPd/C catalyst for hydrogen generation from formic acid at room temperature, *Angew. Chem. Int. Ed.* 52 (2013) 4406–4409.
- [29] L. Dharmarathne, M. Ashokkumar, F. Grieser, Photocatalytic generation of hydrogen using sonoluminescence and sonochemiluminescence, *J. Phys. Chem. C* 116 (2012) 1056–1060.
- [30] D. Lu, G. Yu, Y. Li, M. Chen, Y. Pan, L. Zhou, K. Yang, X. Xiong, P. Wu, Q. Xia, RuCo NPs supported on MIL-96(Al) as highly active catalysts for the hydrolysis of ammonia borane, *J. Alloy. Comp.* 694 (2017) 662–671.
- [31] Z. Zhang, S. Zhang, Q. Yao, X. Chen, Z.-H. Lu, Controlled synthesis of MOF-encapsulated NiPt nanoparticles toward efficient and complete hydrogen evolution from hydrazine borane and hydrazine, *Inorg. Chem.* 56 (2017) 11938–11945.
- [32] H. Dai, J. Su, K. Hu, W. Luo, G. Cheng, Pd nanoparticles supported on MIL-101 as high-performance catalysts for catalytic hydrolysis of ammonia borane, *Int. J. Hydrogen Energy* 39 (2014) 4947–4953.
- [33] L. Zhang, L. Zhou, K. Yang, D. Gao, C. Huang, Y. Chen, F. Zhang, X. Xiong, L. Li, Q. Xia, PdNi nanoparticles supported on MIL-101 as high-performance catalysts for hydrogen generation from ammonia borane, *J. Alloy. Comp.* 677 (2016) 87–95.
- [34] N.-Z. Shang, C. Feng, S.-T. Gao, C. Wang, Ag/Pd nanoparticles supported on amine-functionalized metal–organic framework for catalytic hydrolysis of ammonia borane, *Int. J. Hydrogen Energy* 41 (2016) 944–950.
- [35] B. Xia, C. Liu, H. Wu, W. Luo, G. Cheng, Hydrolytic dehydrogenation of ammonia borane catalyzed by metal–organic framework supported bimetallic RhNi nanoparticles, *Int. J. Hydrogen Energy* 40 (2015) 16391–16397.
- [36] A. Ajiaz, A. Karkamkar, Y.J. Choi, N. Tsumori, E. Ronnebro, T. Autrey, H. Shioyama, Q. Xu, Immobilizing highly catalytically active Pt nanoparticles inside the pores of metal–organic framework: a double solvents approach, *J. Am. Chem. Soc.* 134 (2012) 13926–13929.
- [37] K. Yang, L. Zhou, G. Yu, X. Xiong, M. Ye, Y. Li, D. Lu, Y. Pan, M. Chen, L. Zhang, D. Gao, Z. Wang, H. Liu, Q. Xia, Ru nanoparticles supported on MIL-53(Cr, Al) as efficient catalysts for hydrogen generation from hydrolysis of ammonia borane, *Int. J. Hydrogen Energy* 41 (2016) 6300–6309.
- [38] L. Wen, J. Su, X. Wu, P. Cai, W. Luo, G. Cheng, Ruthenium supported on MIL-96: an efficient catalyst for hydrolytic dehydrogenation of ammonia borane for chemical hydrogen storage, *Int. J. Hydrogen Energy* 39 (2014) 17129–17135.
- [39] W. Zhang, X. Jiang, X. Wang, Y.V. Kaneti, Y. Chen, J. Liu, J.S. Jiang, Y. Yamauchi, M. Hu, Spontaneous weaving of graphitic carbon networks synthesized by pyrolysis of ZIF-67 crystals, *Angew. Chem. Int. Ed.* 56 (2017) 8435–8440.
- [40] K.S. Park, Z. Ni, A.P. Côté, J.Y. Choi, R. Huang, F.J. Uribe-Romo, H.K. Chae, M. O'Keeffe, O.M. Yaghi, Exceptional chemical and thermal stability of zeolitic imidazolate frameworks, *Proc. Natl. Acad. Sci. U. S. A.* 103 (2006) 10186–10191.
- [41] K.-Y.A. Lin, S.-Y. Chen, Catalytic reduction of bromate using ZIF-derived nanoscale cobalt/carbon cages in the presence of sodium borohydride, *ACS Sustain. Chem. Eng.* 3 (2015) 3096–3103.
- [42] X. Yang, H. Li, A.-Y. Lu, S. Min, Z. Idriss, M.N. Hedhili, K.-W. Huang, H. Idriss, L.-J. Li, Highly acid-durable carbon coated Co<sub>3</sub>O<sub>4</sub> nanoarrays as efficient oxygen evolution electrocatalysts, *Nano Energy* 25 (2016) 42–50.
- [43] Y. Zeng, S. Tian, D. Wang, H. Dong, X. Cheng, Y. Zhao, J. Tian, X. Yang, Facile synthesis of polyhedral Pd nanocrystals as a highly active and methanol-tolerant electrocatalyst for oxygen reduction, *ChemistrySelect* 2 (2017) 9291–9297.
- [44] J. Zhang, X. Yang, H. Shao, C.-C. Tseng, S. Tian, W. Hu, C. Jing, J. Tian, Y. Zhao, Microwave-assisted synthesis of Pd oxide-rich Pd particles on nitrogen/sulfur Co-doped graphene with remarkably enhanced ethanol electrooxidation, *Fuel Cell.* 17 (2017) 115–122.
- [45] F. Simescu-Lazar, V. Meille, F. Bornette, F. Campoli, C. de Bellefon, In situ electrochemical regeneration of deactivated coated foam catalysts in a Robinson–Mahoney basket reactor: example of Pd/C for nitrobenzene hydrogenation, *Catal. Today* 249 (2015) 52–58.
- [46] T. Tang, Q. Gan, X. Guo, H. Dong, J. Zhang, Y. Zhao, J. Tian, X. Yang, A hybrid catalyst of Pt/CoNiO<sub>2</sub> on carbon nanotubes and its synergistic effect towards remarkable ethanol electro-oxidation in alkaline media, *Sustain. Energy Fuel.* 2 (2018) 229–236.
- [47] X. Peng, D. Chen, X. Yang, D. Wang, M. Li, C.-C. Tseng, R. Panneerselvam, X. Wang, W. Hu, J. Tian, Y. Zhao, Microwave-assisted synthesis of highly dispersed PtCu nanoparticles on three-dimensional nitrogen-doped graphene networks with remarkably enhanced methanol electrooxidation, *ACS Appl. Mater. Interfaces* 8 (2016) 33673–33680.
- [48] Y. Shi, X. Zhang, Y. Zhu, H. Tan, X. Chen, Z.-H. Lu, Core–shell structured nanocomposites Ag@CeO<sub>2</sub> as catalysts for hydrogenation of 4-nitrophenol and 2-nitroaniline, *RSC Adv.* 6 (2016) 47966–47973.
- [49] W. Wang, Z.-H. Lu, Y. Luo, A. Zou, Q. Yao, X. Chen, Mesoporous carbon nitride supported Pd and Pd–Ni nanoparticles as highly efficient catalyst for catalytic hydrolysis of NH<sub>3</sub>BH<sub>3</sub>, *ChemCatChem* 10 (2018) 1620–1626.
- [50] Q. Yao, K. Yang, X. Hong, X. Chen, Z.-H. Lu, Base-promoted hydrolytic dehydrogenation of ammonia borane catalyzed by noble-metal-free nanoparticles, *Catal. Sci. Technol.* 8 (2018) 870–877.
- [51] I. Hitoshi, D. Hafedih, T. Florencio, M. Hiroki, I. Takayuki, K. Yoshitsugu, Z.S. F., A.-Z. Abdulrahim, A. Yahia, P. Lachezar, Catalytic hydrolysis of sodium borohydride on Co catalysts, *Int. J. Energy Res.* 40 (2016) 2078–2090.
- [52] L. Zhou, J. Meng, P. Li, Z. Tao, L. Mai, J. Chen, Ultrasmall cobalt nanoparticles supported on nitrogen-doped porous carbon nanowires for hydrogen evolution from ammonia borane, *Mater. Horiz.* 4 (2017) 268–273.
- [53] L. Cui, Y. Xu, L. Niu, W. Yang, J. Liu, Monolithically integrated CoP nanowire array: an on/off switch for effective on-demand hydrogen generation via hydrolysis of NaBH<sub>4</sub> and NH<sub>3</sub>BH<sub>3</sub>, *Nano Res.* 10 (2017) 595–604.
- [54] X. Huang, D. Wu, D. Cheng, Porous Co<sub>2</sub>P nanowires as high-efficient bifunctional catalysts for 4-nitrophenol reduction and sodium borohydride hydrolysis, *J. Colloid Interface Sci.* 507 (2017) 429–436.
- [55] A. Koska, N. Toshikj, S. Hoett, L. Bernaud, U.B. Demirci, Volcano plot for bimetallic catalysts in hydrogen generation by hydrolysis of sodium borohydride, *J. Chem. Educ.* 94 (2017) 1163–1166.